JOURNAL OF MATERIALS SCIENCE **36** (2001) 4377–4384

Properties of zinc sulphide nanoparticles stabilized in silica

N. HEBALKAR
R&DE (Engrs), Dighi, Pune 411 015, India

A. LOBO
Department of Physics, University of Pune, Pune 411 007, India

S. R. SAINKAR, S. D. PRADHAN
National Chemical Laboratory, Pashan, Pune 411 008, India

W. VOGEL, J. URBAN
Fritz Haber Institut der Max Planck Gesellschaft, Faradayweg 4-6, D-14195 Berlin, Germany

S. K. KULKARNI
Department of Physics, University of Pune, Pune 411 007, India
E-mail: skk@physics.unipune.ernet.in

Zinc sulphide nanoparticles have been synthesized in silica matrix using sol-gel method. It is observed that silica could be loaded with zinc sulphide over a very wide range of concentration without changing the nanoparticle size. A strongly luminescent zinc sulphide-silica composite, thermally stable even upto ~700°C was thus obtained. Several techniques like UV absorption, photoluminescence, x-ray diffraction, scanning electron microscopy, transmission electron microscopy, thermogravimetry and photoelectron spectroscopy have been performed to analyse the ZnS-silica composites.

1. Introduction

Nanoparticles have been extensively investigated during the last decade due to their unique properties and application potential [1–5]. Nanoparticles can be considered as intermediates between molecules and solids. However, molecules have definite dimensions and well-defined properties. Extended solids also possess well-defined properties but the properties do not depend upon the size. Nanoparticles on the other hand are characterized by size dependent properties. In fact, all the materials whether metals, semiconductors or insulators exhibit size dependent properties when some characteristic size of that material is approached. For most of the materials this size is less than 100 nm. Obviously surface to bulk atom ratio also increases dramatically when such nanometric dimensions are reached. Indeed, for nanoparticles, size and surface effects are both important. By controlling these, it is possible, in principle, to design materials of required optical, magnetic, elastic, chemical etc. properties. A large number of synthesis routes like cluster deposition, embedding the particles in zeolites, glass or polymers, electrodeposition, sol-gel synthesis, sonochemical synthesis, chemical capping etc have been devised [1, 2] to achieve materials of desired properties and new methods are continuously being devised. There are, however, challenges resulting from the requirement of stability of the particles as well as narrow size distribution.

Semiconductor nanoparticles are particularly interesting due to their possible applications in diverse areas such as photocatalysis, solar cells, display panels and new devices like single electron transistors and so on [6–8]. Since the earlier work by Efros and Efros [9] and Brus [3] it has been appreciated that size dependent properties in semiconductor materials are possible as the particle size approaches the Bohr radius of the exciton. This requirement is basically attributed to the confinement of charged particles within the small volume of the particle and is known as the quantum size effect (QSE) or quantum confinement effect (QCE). The Bohr radius of the exciton in semiconductors is extremely small. Consequently the number of surface atoms becomes quite large and affects the thermodynamical properties like melting point or phase transition etc [10, 11]. In semiconductor nanoparticles the QSE also results in size dependent energy gaps and changes in the quantum efficiency for luminescence [8, 12].

It is essential to synthesize semiconductor nanoparticles not only with a narrow size distribution but also with good thermal stability. In many cases semiconductor nanoparticles are synthesized in polymers, using the chemical capping method or by embedded them in an inert matrix. Such a matrix is useful in avoiding the coalescence of the nanoparticles. However an organic matrix can provide stability only upto some medium temperature range less than ~300°C [13–15]. The

matrix in which particles are embedded can affect the observed properties of the particles due to a changed local field at the boundary. It is therefore essential that some composite materials are produced that will combine the advantageous properties of the quantum size effect in semiconductors as well as provide adequate thermal stability and give mechanical support to the nanoparticles.

In previous work [13–17] chemically capped zinc sulfide and cadmium sulfide nanoparticles showing the quantum size effect were synthesised and their structural and optical properties were investigated. Chemical capping of organic molecules provided chemical stability upto ~300°C [14, 15]. However, beyond this temperature the particles coalesce. Although synthesis of semiconductor nanoparticles in glass is a good method of giving thermal stability to the nanoparticles along with rigid matrix support, the loading of nanoparticles is usually quite low (<5%). Therefore zinc sulfide nanoparticles in a silica matrix have been synthesised using a simple and inexpensive procedure different to the methods reported earlier by Tan *et al*. [18] and Dhas *et al*. [19]. A loading of ~60% ZnS is achieved by this technique. The composites so formed have been investigated by a variety of techniques such as x-ray diffraction (XRD), thermogravimetry (TG), transmission electron microscopy (TEM), scanning electron microscopy (SEM) and x-ray photoelectron spectroscopy (XPS). These investigations show that good quality ZnS nanoparticles of high thermal stability, especially suitable as a blue phosphor material can be synthesized by a relatively simple method.

2. Experimental

Zinc sulfide nanoparticles were synthesized by a sol-gel method as follows. Hydrolysis of Tetraethylorthosilicate (TEOS) was carried out by adding TEOS : Ethanol : H_2O : HCl in 1 : 4 : 4 : 0.068 molar ratios. Although a large number of samples with varying molarity were synthesized, only three samples i.e. without ZnS (***A***), with a low concentration of ZnS (***B***) and a large concentration of ZnS (***C***) are discussed here. The solution was mixed thoroughly for thirty minutes at room temperature. Zinc acetate of predetermined molarity was then added and the solution was stirred again. Finally Na_2S of required molarity was added and the solution was vigorously stirred again for approximately ninety minutes. The solution was then transferred to the glass vials for gelation. Gelation occurred within about an hour. Samples were left in glass vials at room temperature for drying. The gels were completely dried in 7 days and opaque samples of zinc sulfide embedded in a silica matrix were obtained. The samples without zinc sulfide were transparent but transparency reduced with increasing zinc sulfide content. The samples were quite hard and handleable.

The Morphology of the samples was observed using a Leica Cambridge Stereoscan S-440 Scanning Electron Micrograph (SEM) supplied by M/S Leica Cambridge Ltd. UK. As the samples are highly insulating, they were coated by gold using a Poloran E5000 sputter coating unit using 20 kV and 25 pA current. The microscope is equipped with a 35 mm camera attached to high resolution recording unit.

TEM was performed using a Philips CM200 FEG microscope equipped with a field emission gun. An accelerating voltage of 200 kV was used. Samples were dispersed in ethanol and a drop of the solution was placed on an amorphous carbon film ~5 nm thick. After the liquid evaporated, the samples could be introduced into the microscope.

X-ray diffraction analysis of the samples was carried out using a Guinier powder diffractometer (Huber) using Cu K_{α_1} radiation. Samples were sandwiched between 3 mm polyethylene foils for these experiments. All the patterns are corrected by subtracting the signal of the pure SiO_2 carrier and the foil that produces a characteristic background pattern of an amorphous substance.

Optical absorption was carried out in the UV range (200 nm to 500 nm) using a Shimatzu UV 300 model double beam spectrophotometer. The samples were dispersed in double distilled water for this analysis.

For the photoluminescence studies (PL), a Perkin Elmer model LS-50 with Xe flash lamp as the source of excitation was used. Excitation and emission spectra were recorded in the fluorescence mode over a range of 250 nm to 700 nm.

Presence of zinc sulfide in the samples was determined using x-ray photoelectron spectroscopy. ESCA LAB MK II set up supplied by Vacuum Generators Ltd. U.K. was used for this. A Mg K_α ($h\nu$ 1253.6 eV) x-ray source with concentric hemispherical analyser (CHA) operated at 50 eV pass energy resulted into a total resolution of 1.0 eV. $Au4f_{7/2}$ at 84.0 eV was used as an external reference and Cls at 285.0 eV as an internal standard.

The thermal stability was checked using thermogravimetry (TG/DTA-32 M/S Sieko). The temperature range was from 30°C to 1000°C with a heating rate of 10°C/min. The experiments were carried out in a nitrogen atmosphere.

3. Results and discussion

For a long time, zinc sulfide has been known to be a phosphor material. Therefore pure, as well as doped, zinc sulfide nanoparticles have been extensively investigated [8, 20–22] in order to explore the possibility of using nanoparticles as better phosphor materials. However, little seems to have been discussed regarding the thermal stability of these particles, which is quite important from their application point of view.

Using the experimental procedure described above, it was possible to synthesize ZnS-silica composites with different ZnS loading.

Several trends have been noticed with increased loading of ZnS. Fig. 1a–c shows SEM photographs of three typical samples. It can be seen that with increasing ZnS concentration a rough surface is formed. A dense ZnS film on silica for sample ***C*** is evident in Fig. 1c.

X-ray diffraction analysis of the samples shows that silica has an amorphous network and the crystallanity

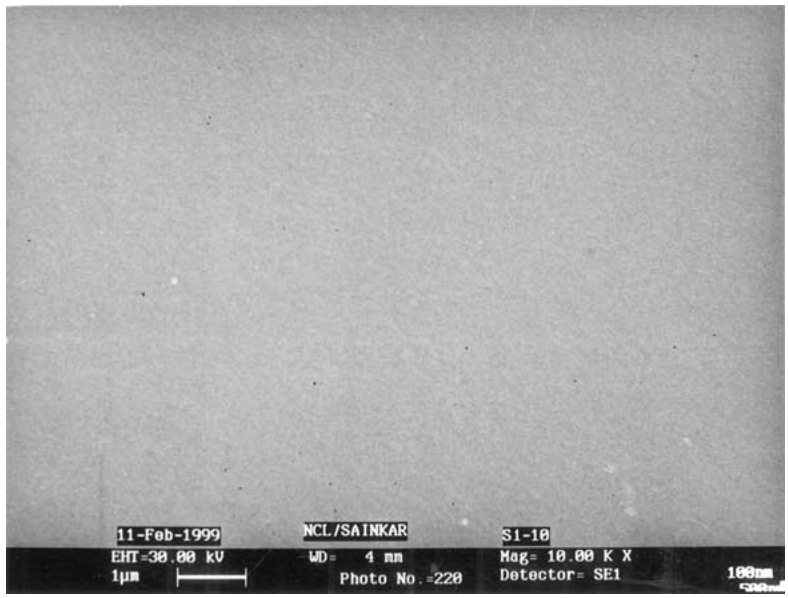

(a)

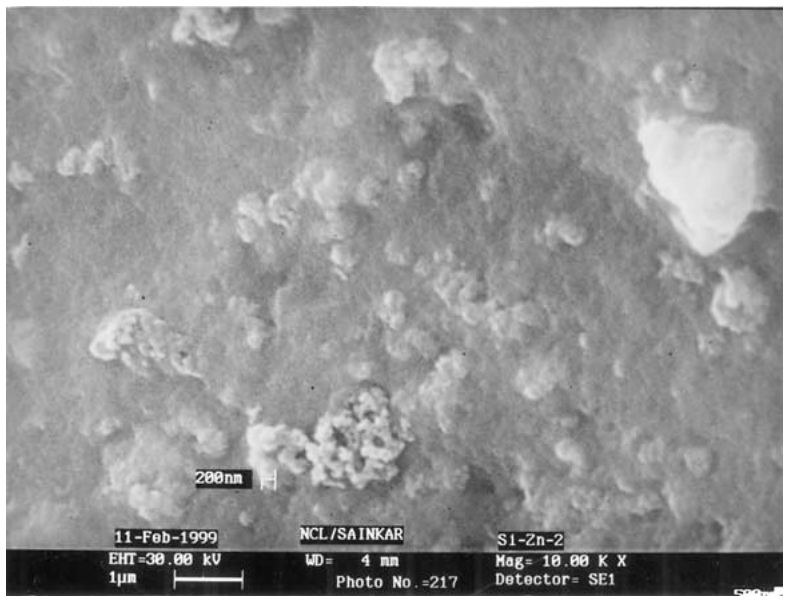

(b)

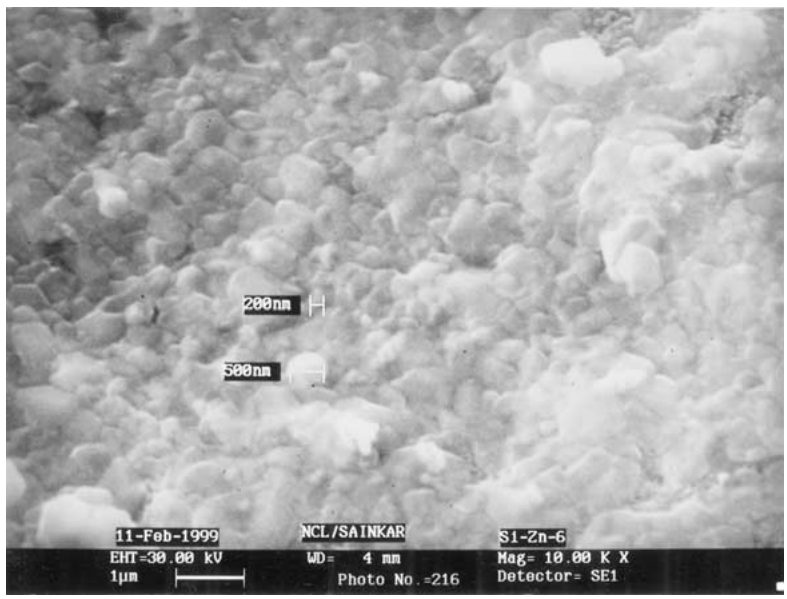

(c)

Figure 1 SEM photomicrographs of silica sample ***A***, (a) ZnS-silica composite sample ***B***, (b) and ZnS-silica composite sample ***C***. (c)

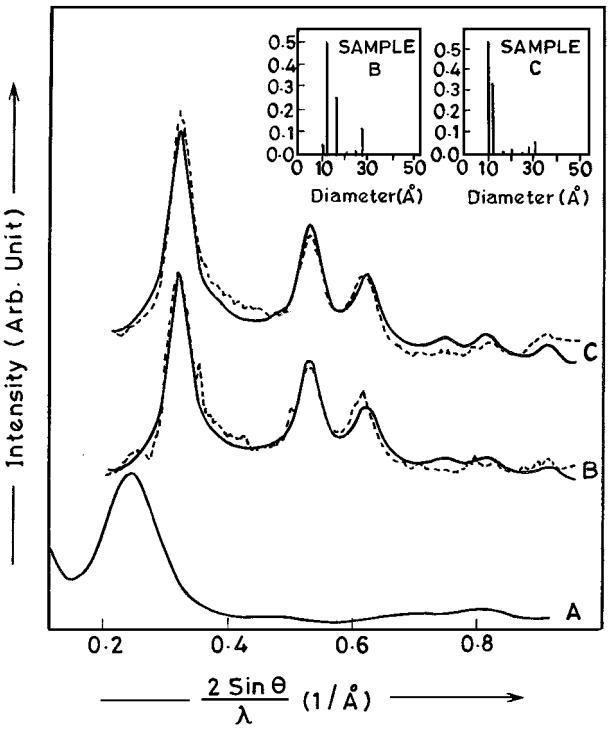

Figure 2 Wide angle x-ray diffraction patterns of samples ***A***, ***B*** and ***C***. The ____ shows in each case the experimental curve and --- indicates the fitted curves according to the Debye Function Analysis (DFA). The inset depicts the size distribution of cubic particles predicted from DFA analysis.

of the ZnS-silica composites is apparent from Fig. 2. Strong diffraction peaks produced for samples ***B*** and ***C*** are due to the ZnS nanoparticles. Debye Function Analysis (DFA) of the diffraction patterns were used for the ZnS-silica composites. DFA analysis can give [22, 23] information about particle sizes and their distribution. It can also provide information about different phases in the samples if present. This method was used for capped nanoparticles of ZnS and CdS [13, 14]. The inset in Fig. 2 shows the size distribution of ZnS particles in samples ***B*** and ***C***. It can be seen that in both cases the maximum particle size is around 1.2 nm. Also this analysis shows that the particles are cubic in structure. However, TEM analysis showed that together with cubic particles, a few hexagonal particles were observed. In Fig. 3a–d examples of cubic and hexagonal particles for samples B and C are displayed, respectively. The power spectra, i.e. squares of the Fourier transforms of the images are also shown next to the images. Fig. 3a and c are cubic particles in the [110]- and [111]-orientation for samples B and C. Fig. 3b and d are the corresponding hexagonal structures both in the [001]-orientation for the two different samples.

It can be seen from the power spectra that the corresponding netplane spacings for the cubic structures are in very good agreement with bulk sphalerite. The displayed reflections for the particle in the [110]-orientation are $2\,\bar{2}\,0$, $1\,\bar{1}\,1$ and $\bar{1}\,1\,1$ with spacings of 0.194 nm, 0.319 nm and 0.313 nm respectively. The bulk data are 0.191 nm, 0.312 nm and 0.312 nm. For the particle in the [111]-orientation the reflections are $0\,\bar{2}\,2$, $\bar{2}\,0\,2$ and $\bar{2}\,2\,0$ with spacings of 0.201 nm for each spacing. The bulk data are again 0.191 nm. However, the spacings of hexagonal particles are up to 14% smaller than bulk wurtzite. The reflections in both [001]-orientations are $\bar{1}\,1\,0$, $0\,1\,0$ and $1\,0\,0$ with spacings of 0.303 nm, 0.294 nm and 0.289 nm for sample B and 0.288 nm for all three spacings of sample C. The data of bulk wurtzite are 0.332 nm.

It was not possible to obtain the statistical distribution of cubic and hexagonal particles using TEM. However, the DFA analysis shows that the crystals are cubic. It is likely that only bigger particles were picked up by the TEM analysis. These were hexagonal and cubic so it is possible that a large number of particles which were smaller in size were mostly cubic. In the present case it was not possible to detect particles smaller than ~2 nm using TEM. It can be concluded that mostly cubic ZnS particles are present in both the samples ***B*** and ***C***.

UV absorption analysis of the samples also provides information relating to the size of the particles. It can be seen from Fig. 4 that there is a peak at ~300 nm. The band gap of bulk ZnS is 3.6 eV. The onset of absorption is located at 340 nm. It is not possible to observe any excitonic peak in the room temperature absorption spectra. Due to the QSE there is a blue shift in the absorption and a strong excitonic peak also appears [3] at ~300 nm. It is noticed that with increasing loading the position of the excitonic peak does not shift. This implies that the particles do not coalesce as the ZnS loading increases. This is because all the particles are covered with silica and retain their small sizes. Under the given conditions of pH and concentrations of chemicals, a narrow size distribution of particles was possible.

Further support to these arguments comes from the PL observations. Fig. 5 shows the PL spectra for low and high ZnS loadings. It is known that for ZnS, blue luminescence around 400 nm occurs even for nanoparticles [5]. Nanoparticles are not completely free of defects. In fact it has been shown recently that [14] in the case of ZnS that defects are present even in small particles. Thus blue luminescence in the case of ZnS nanoparticles is attributable to the defects in them. The only change in the case of nanoparticles that can occur is the change in the luminescence decay time. As suggested by Bhargava *et al.* [12] overlap of electron hole wave functions in nanoparticles may result in a change in the luminescence decay time and the quantum efficiency for luminescence may increase. This view has been challenged recently [24, 25]. However more work will be required to understand this problem. The nature of excitation and emission spectra is similar for all the loadings except for the increase in intensity with increase in ZnS loading. However excitation peaks for both the samples ***B*** and ***C*** are at the same position i.e. 350 nm and emission peaks are at ~400 nm. A similar situation is found for all other loadings of ZnS. It was, however, seen that blue photoluminescence from ZnS-silica composites was much stronger than for the organic molecule capped ZnS. In Fig. 6 the increase in PL intensity with ZnS loading is illustrated. In the small ZnS loading region there is a linear increase in PL intensity which rapidly tends to saturate. This is possible

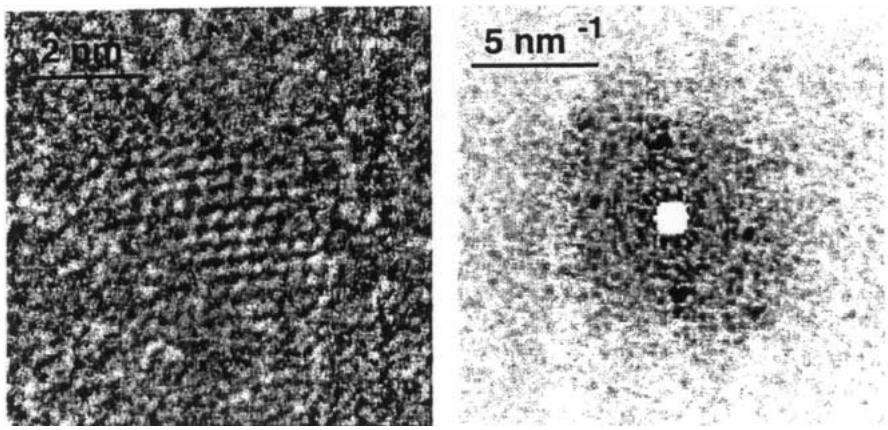

(a)

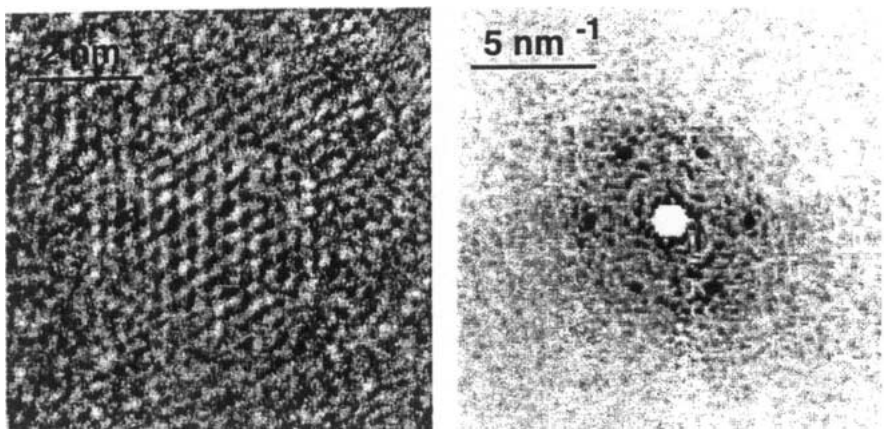

(b)

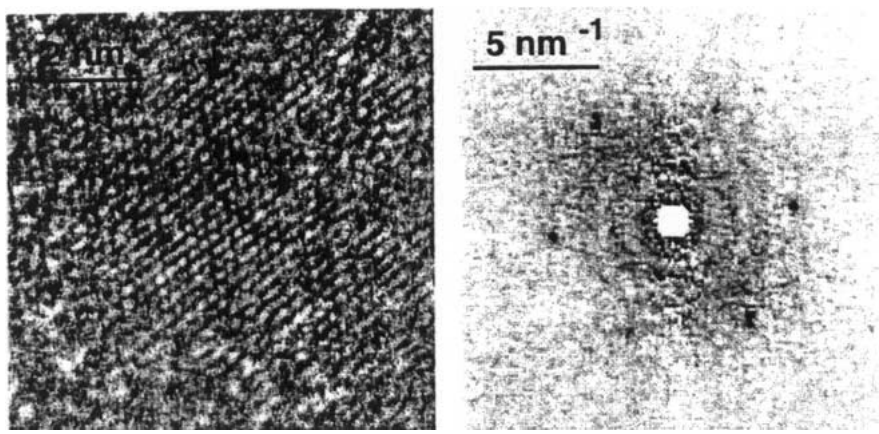

(c)

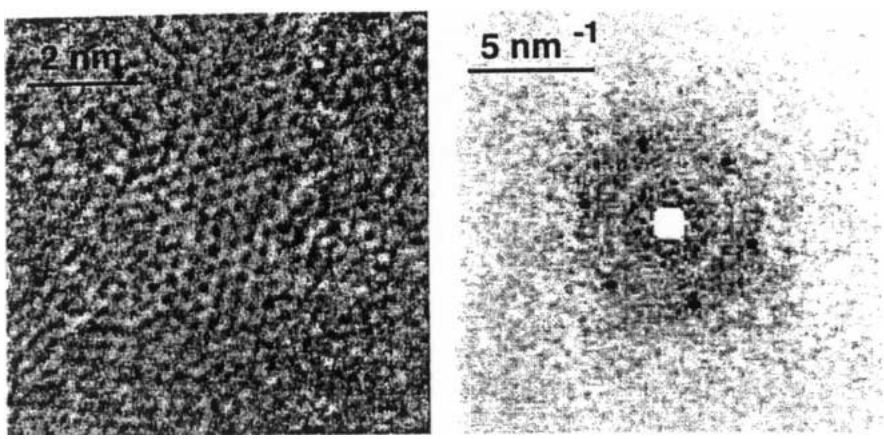

(d)

Figure 3 TEM Photo Micrographs of ZnS particles. Corresponding power spectra also are illustrated. (a) Sample B, cubic particle in the [110]-orientation. (b) Sample B, hexagonal particle in the [001]-orientation. (c) Sample C, cubic particle in the [111]-orientation. (d) Sample C, hexagonal particle in the [001]-orientation.

TABLE I Binding energy values of various core levels and atomic concentrations of samples determined using x-ray photoelectron spectroscopy

	Sample A		Sample B		Sample C	
Elements	Binding energy (eV)	Atomic concentration	Binding energy (eV)	Atomic concentration	Binding energy (eV)	Atomic concentration
Si	103.8	39.82	103.5	28.38	103.5	16.95
O	533.2	50.54	533.0	51.22	533.0	26.78
C	285.0	9.63	285.0	8.36	285.0	18.66
Zn	–	–	1022.6	3.19	1022.6	11.56
S	–	–	161.5	3.90	161.5	14.42
Na	–	–	1072.5	4.92	1072.5	11.60
Zns : SiO_2	–		0.088		0.59	

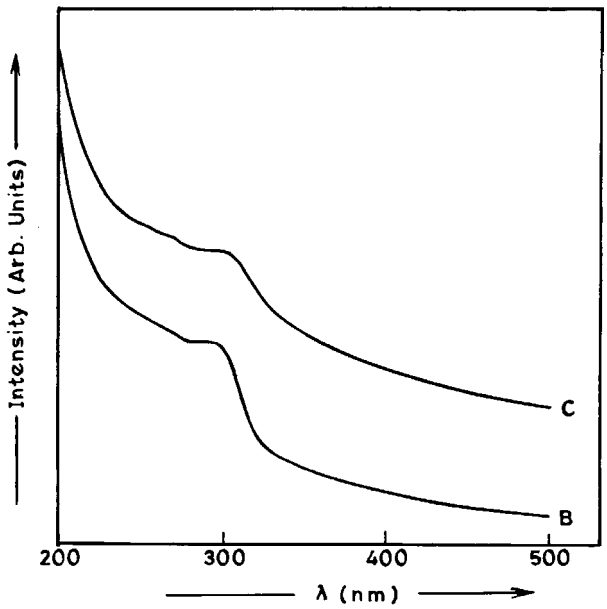

Figure 4 UV absorption spectra of samples B and C dispersed in double distilled water.

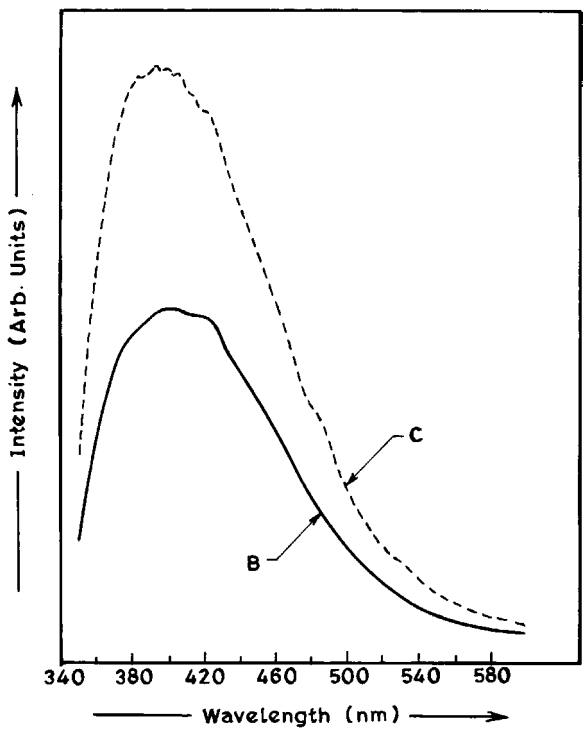

Figure 5 Photoluminescence spectra from samples ***B*** and ***C***.

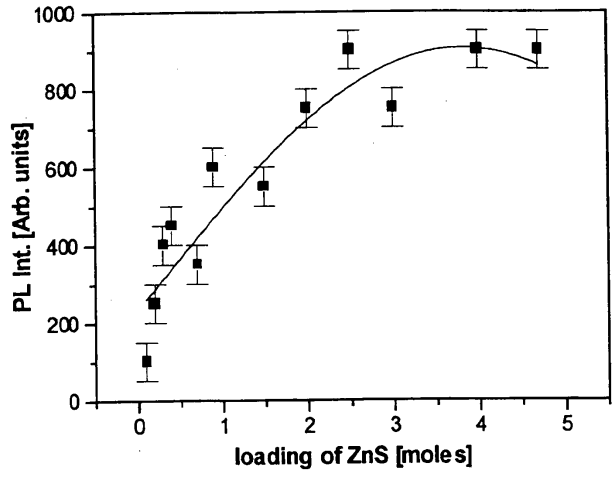

Figure 6 Photoluminescence intensity as a function of ZnS loading.

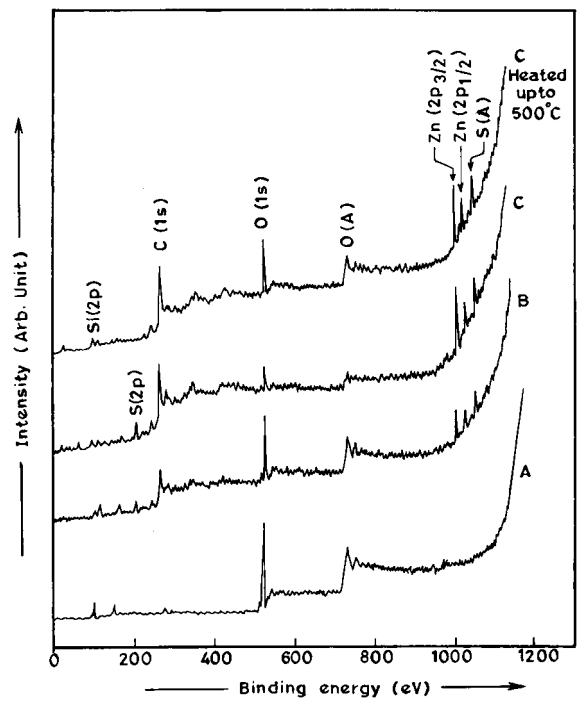

Figure 7 XPS survey scans for samples ***A***, ***B***, & ***C*** and sample ***C*** heated upto 500°C for 30 minutes.

as PL intensity is due to only a small region (~0.1 μm) from the sample surface of a thick sample.

Further the composition of the ZnS-silica matrix composites has been investigated using x-ray photoelectron spectroscopy. Fig. 7 depicts the survey

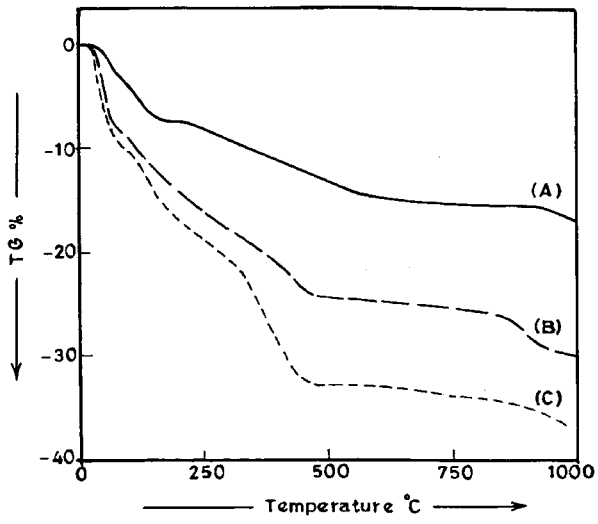

Figure 8 Thermogravimetry results from samples ***A***, ***B***, & ***C***. Samples were heated in a nitrogen atmosphere at a rate of 10°C min^{-1}.

scans for samples **A**, **B** and **C** at room temperature. Photoemission lines corresponding to Zn, S, Si, C, O and Na were detected. Table I lists the atomic concentrations of various elements present as well as their binding energies. ZnS/SiO_x ratios are also listed. The ZnS/SiO_x ratio for sample **B** is ∼0.088 and that for sample **C** is ∼0.59. If the carbon in the samples is neglected and just the proportion of ZnS with respect to SiO_x is considered then sample **B** has 8.8% ZnS and sample **C** has ∼59% ZnS. Thus changes in the ZnS concentration indeed take place from sample to sample. It can be seen that binding energies for Zn and S are in the range of those observed for bulk ZnS. Sample **C** was in-situ heated in ultra high vacuum (UHV) at 500°C for 30 min. to check if ZnS was still retained in the sample. UHV was used to avoid the oxidation and contamination of the ZnS sample. A loss of 31% ZnS takes place. Unfortunately further in-situ heating of the sample was not possible.

In order to further investigate the thermal stability of the samples, **A**, **B** and **C** were subjected to thermogravimetry analysis. From Fig. 8 it can be seen that, at 1000°C, weight loss in sample A is ∼16%. In sample B and C it is ∼29% and ∼37% respectively. The rate of weight loss is rapid till 450°C. Between 450°C and 1000°C the weight loss is less. Initially, upto 100°C, the weight loss may be partially due to evaporation of moisture present in the sample. Above this temperature some ZnS may be evaporating. The pure silica sample is the most stable and weight loss increases with increasing ZnS content. However, ZnS is not completely lost even at 500°C. This is clear from two observations: (i) The PL spectra do not lose intensity completely even at 500°C and (ii) XPS spectra also show the presence of ZnS in the sample heated to this temperature. Fig. 9 shows the PL due to sample **C**, heated at various temperatures in a nitrogen atmosphere. All the spectra show peaks around 350 nm wavelength. As can be seen, the spectrum due to the sample at R.T. is intense and broad. Such a broad peak is characteristic of various defect centres present in the band gap of the ZnS nanoparticles. Denzler *et al.* [26] have surveyed a series of ZnS

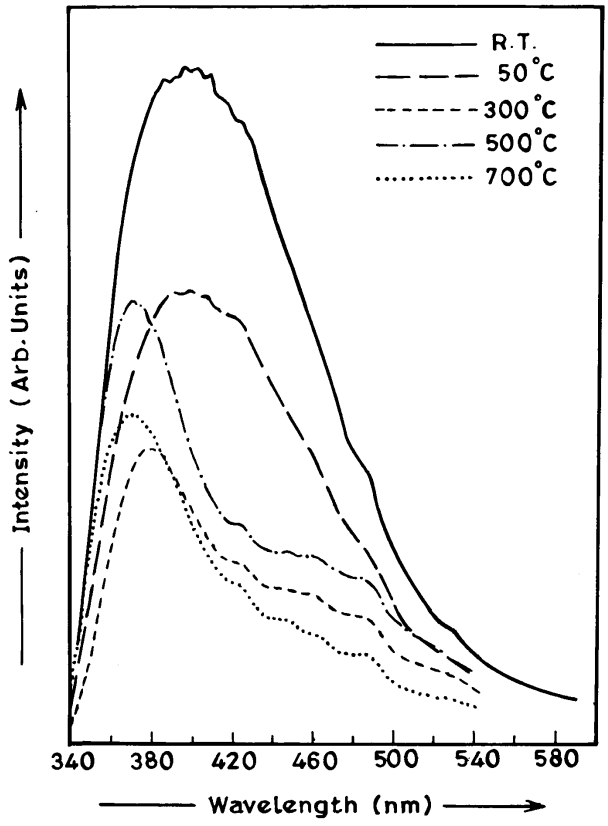

Figure 9 Photoluminescence spectra from sample ***C*** at various temperatures. The excitation wavelength in all the cases was fixed at 320 nm.

nanocrystal samples and obtained different spectra in the 400–800 nm range. They have fitted four components arising due to defects in the energy gaps of ZnS in the range of 400–800 nm. These are all point defects contributed by interstitial sulphur (416.1 nm), interstitial zinc (423.9 nm), sulphur vacancy (430.1 nm) and zinc vacancy (437.18 nm). Although exact peak positions are not be same (in the present case all the spectra are shifted to lower wavelength, possibly from changes in the calibration or sample preparation), reduction in intensity of PL peaks with sample heating indicates that zinc and sulphur vacancies may be responsible for the observed PL spectra. Heating of the sample to 50°C reduces the PL intensity but the spectral width is still large. Heating the sample to 300°C reduces the intensity as well as the width of the spectrum. The peak is at 380 nm instead of ∼400 nm. This indicates that some of the defects are annealed out. Heating to 500°C increases the intensity of the peak at 380 nm. It is likely that the defect density has increased. Also a small shift in peak maximum to 370 nm is observed. However again at 700°C the spectral intensity is reduced. This is due to loss of ZnS from the sample as confirmed from TG analysis.

4. Conclusions

Highly stable nanoparticles of ZnS in silica have been synthesized. It was possible to load the silica with various amounts of ZnS without changing the particle size. The stability of ZnS in this matrix is good. The defects present in the ZnS are responsible for the a strong blue luminescence; their density changes with heating.

Acknowledgement

NH would like to thank R&DE (Engrs), Pune for the fellowship and SKK thanks UGC India for the continuous support.

References

1. R. UYEDA, *Prog. Mat. Sci.* **35** (1991) 1.
2. H. GLEITER, *ibid.* **33** (1989) 223.
3. L. E. BRUS, *J. Chem. Phys.* **79** (1983) 5566.
4. A. P. ALIVISATOS, *Science* **271** (1996) 933.
5. A. HENGLEIN, *Topics in Curr. Chem.* **143** (1988) 113.
6. D. L. KLEIN, R. ROTH, A. K. LIM, A. P. ALIVISATOS and P. MCEUEN, *Nature* **389** (1997) 699.
7. V. L. COLVIN, M. C. SCHLAMP and A. P. ALIVISATOS, *ibid.* **370** (1994) 354.
8. R. N. BHARGAVA, *J. Lum.* **70** (1996) 85.
9. AL. L. EFROS and AL. EFROS, *Sov. Phys. Semicond.* **16** (1982) 772.
10. A. N. GOLDSTAIN, C. M. ECHER, and A. P. ALIVISATOS, *Science* **256** (1992) 1425.
11. A. P. ALIVISATOS, *J. Phys. Chem.* **100** (1996) 13226.
12. R. N. BHARGAVA, D. GALLAGHER, X. HONG and A. NURMIKKO, *Phys. Rev. Lett.* **72** (1994) 416.
13. W. VOGEL, J. URBAN, M. KUNDU and S. K. KULKARNI, *Langmuir* **13** (1997) 827.
14. W. VOGEL, P. H. BORSE, N. DESHMUKH and S. K. KULKARNI, *ibid.* **16** (2000) 2032.
15. U. WINKLER, D. EICH, Z. H. CHEN, R. FINK, S. K. KULKARNI and E. UMBACH, *Phys. Stat. Solidi* **173** (1997) 253.
16. M. KUNDU, A. A. KHOSRAVI, P. SING and S. K. KULKARNI, *J. Mater Sci.* **32** (1997) 245.
17. U. WINKLER, D. EICH, Z. H. CHEN, R. FINK, S. K. KULKARNI and E. UMBACH, *Chem. Phys. Lett.* **306** (1999) 95.
18. MING TAN, WEIPING CAI and LIDE ZHANG, *Appl. Phys. Lett.* **71** (1997) 3697.
19. N. ARUL DHAS, A. ZABAN and A. GEDANKEN, *Chem. Mater.* **11** (1999) 806.
20. A. A. KHOSRAVI, M. KUNDU, G. S. SHUKHAWAT, R. P. GUPTA, A. K. SHARMA, P. D. VYAS and S. K. KULKARNI, *Appl. Phys. Lett.* **67** (1995) 2506.
21. A. A. KHOSRAVI, M. KUNDU, L. JATWA, S. K. DESHPANDE, V. A. BHAGVAT, M. SASTRI and S. K. KULKARNI, *ibid* **67** (1995) 2702.
22. V. GNUTZMANN and W. VOGEL, *J. Phys. Chem.* **94** (1990) 4991.
23. W. VOGEL, B. ROSNER, and B. TESCHE, *ibid.* **97** (1993) 11611.
24. A. A. BOL and A. MEIJERINK, *Phys. Rev. B* **58** (1998) R15997.
25. S. K. KULKARNI, *Appl. Surf. Sci.* (in press).
26. D. DENZLER, M. OLSCHEWSKI and K. SATTLER, *J. Appl. Phys.* **84** (1998) 2841.

Received 1 September 2000
and accepted 21 April 2001